THE JOURNAL OF BIOLOGICAL CHEMISTRY VOL. 288, NO. 37, pp. 26616–26624, September 13, 2013

Identification, Structure, and Function of a Novel Type VI Secretion Peptidoglycan Glycoside Hydrolase Effector-Immunity Pair*[S]

Received for publication, May 27, 2013, and in revised form, June 18, 2013 Published, JBC Papers in Press, July 22, 2013, DOI 10.1074/jbc.M113.488320

John C. Whitney[‡], Seemay Chou[‡1], Alistair B. Russell[‡2], Jacob Biboy[§], Taylor E. Gardiner[‡3], Michael A. Ferrin[‡3], Mitchell Brittnacher[¶], Waldemar Vollmer[§4], and Joseph D. Mougous[‡§5]

From the Departments of [‡]Microbiology and [¶]Immunology, University of Washington, Seattle, Washington 98195 and [§]Centre for Bacterial Cell Biology, Institute for Cell and Molecular Biosciences, Newcastle University, Newcastle upon Tyne NE2 4HH, United Kingdom

Background: The bacterial type VI secretion system (T6SS) translocates toxic effector proteins into target cells.
Results: Novel T6S peptidoglycan glycoside hydrolase effector-immunity families are identified and a representative pair is structurally and functionally characterized.
Conclusion: Peptidoglycan glycoside hydrolase effectors are an important component of the T6S effector arsenal.
Significance: This work expands the repertoire of known T6S substrates and reports the first structure of a peptidoglycan glycoside hydrolase effector.

Bacteria employ type VI secretion systems (T6SSs) to facilitate interactions with prokaryotic and eukaryotic cells. Despite the widespread identification of T6SSs among Gram-negative bacteria, the number of experimentally validated substrate effector proteins mediating these interactions remains small. Here, employing an informatics approach, we define novel families of T6S peptidoglycan glycoside hydrolase effectors. Consistent with the known intercellular self-intoxication exhibited by the T6S pathway, we observe that each effector gene is located adjacent to a hypothetical open reading frame encoding a putative periplasmically localized immunity determinant. To validate our sequence-based approach, we functionally investigate a representative family member from the soil-dwelling bacterium *Pseudomonas protegens*. We demonstrate that this protein is secreted in a T6SS-dependent manner and that it confers a fitness advantage in growth competition assays with *Pseudomonas putida*. In addition, we determined the 1.4 Å x-ray crystal structure of this effector in complex with its cognate immunity protein. The structure reveals the effector shares highest overall structural similarity to a glycoside hydrolase family associated with peptidoglycan *N*-acetylglucosaminidase activity, suggesting that T6S peptidoglycan glycoside hydrolase effector families may comprise significant enzymatic diversity. Our structural analyses also demonstrate that self-intoxication is prevented by the immunity protein through direct occlusion of the effector active site. This work significantly expands our current understanding of T6S effector diversity.

Bacteria utilize specialized protein secretion systems to mediate interactions with organisms in their environment. The bacterial type VI secretion system (T6SS)[6] is a multi-protein apparatus that translocates substrate effector proteins into neighboring Gram-negative bacterial cells (1–3). Many of these proteins act as toxins; thus, their delivery grants the donor bacterium fitness in co-culture with susceptible competitors. Although the precise mechanism of effector translocation by the T6SS remains unclear, data indicate that effectors are delivered in single step from the cytoplasm of a donor bacterium to the periplasm of a recipient (3). Structural similarity between secreted T6S apparatus components and bacteriophage proteins involved in cell puncturing suggest that the translocation process may resemble phage infection (4, 5).

In recent years, significant progress has been made toward the identification and functional characterization of antibacterial effectors secreted by the T6SS. Bacteria-targeting effectors associated with T6S have been shown to elicit toxicity through the disruption of a variety of cellular structures including nucleic acids (6), membranes (7, 8), and the bacterial cell wall (3, 9–11). For example, the RhsA (recombination hot spot A) and RhsB proteins of *Dickeya dadantii* contain C-terminal toxin domains that degrade chromosomal DNA (6), and Tle (type VI secretion lipase effector) proteins from *Vibrio cholerae*, *Burkholderia thailandensis*, and *Pseudomonas aeruginosa* are lipases that catalyze the breakdown of membrane phospholipids (7). Cell wall-degrading T6S effectors distribute into two

* This work was supported by National Institutes of Health Grant AI080609.
The atomic coordinates and structure factors (code 4KT3) have been deposited in the Protein Data Bank (http://wwpdb.org/).
[S] This article contains supplemental Figs. S1–S3.
[1] Supported by a Howard Hughes Medical Institute Life Sciences Research Foundation Fellowship.
[2] Supported by a Graduate Research Fellowship from National Science Foundation Grant DGE-0718124.
[3] Supported by Mary Gates Undergraduate Research Scholarships.
[4] Supported by the Biotechnology and Biological Sciences Research Council (BB/I020012/1).
[5] An investigator in the Pathogenesis of Infectious Disease Award from the Burroughs Wellcome fund. To whom correspondence should be addressed: Dept. of Microbiology, University of Washington, Seattle, WA 98195. Tel.: 206-685-6740; E-mail: mougous@u.washington.edu.

[6] The abbreviations used are: T6SS, bacterial type VI secretion system; MurNAc, *N*-acetylmuramic acid; GlcNAc, *N*-acetylglucosamine; E-I, effector-immunity; LB-LS, Luria-Bertani low salt; IPTG, isopropyl 1-thio-β-D-galactopyranoside; ITC, isothermal titration calorimetry; G-type, goose-type.

groups: those that act as amidases, cleaving the peptidoglycan molecule within its peptide stems and cross-links and those that act as glycoside hydrolases, cleaving the glycan backbone of the molecule. T6S amidase effectors have been studied extensively (3, 9, 10, 12–15). The enzymes are broadly distributed among Proteobacteria and form four phylogenetically distinct families that constitute the Tae (type IV secretion amidase effector) superfamily. Interestingly, the preferred cleavage site within peptidoglycan can vary between Tae families, suggesting the possibility that optimal effector specificity is dependent on the organism(s) targeted and/or the precise structure of the peptidoglycan found in those organisms.

In contrast to the amidases, there are few identified glycoside hydrolase cell wall-targeting effectors. Moreover, the general utilization of this effector activity by T6SS$^+$ organisms remains uncertain. *P. aeruginosa* Tse3, the sole biochemically characterized glycoside hydrolase effector, acts as a muramidase, cleaving the β-(1,4) linkage between *N*-acetylmuramic acid (MurNAc) and *N*-acetylglucosamine (GlcNAc) (3). The only other glycoside hydrolase effector identified to date is VgrG-3 from *V. cholerae*. This protein carries a C-terminal lysozyme-like effector domain that degrades peptidoglycan (3, 11, 16).

A commonality among all identified effectors with antibacterial activity is that their corresponding open reading frames are found adjacent to genes encoding cognate immunity proteins. These proteins confer immunity by specifically binding to and inactivating their associated effector (3, 13–15). As effectors do not access the donor cell periplasm in transit to the recipient cell, the immunity proteins of cell wall-targeting effectors, which reside in the periplasm, serve the exclusive purpose of preventing intercellular self-intoxication.

The sequence divergence and sporadic distribution of T6S effectors present a challenge for the identification of these important mediators of interbacterial interactions. Owing to their frequent horizontal inheritance, bacteria related at the genus, or even the species level, often contain a completely unique repertoire of these proteins. For example, the plant commensal bacterium *Pseudomonas protegens* does not contain homologs of the three established effectors of the *P. aeruginosa* Hcp secretion island I-encoded T6SS (H1-T6SS), Tse1–3; however, this organism possesses a T6SS orthologous to the H1-T6SS (17).

One way in which the challenge of identifying T6SS effectors has been overcome is by exploiting the tendency of their corresponding genes to reside within or in close proximity to T6SS-encoding gene clusters. This approach was used for the identification of Tae4 family members from *Serratia marcescens* (12). Alternatively, mass spectrometry-based methodologies have been successful in the identification of T6S effectors from *P. aeruginosa*, *Burkholderia thailandensis*, and *S. marcescens* (2, 9, 18). Finally, our group utilized a sequence homology-independent informatic search based on common properties found within effector-immunity (E-I) pairs to identify the Tae superfamily (9). These properties, applied independently to the candidate effector and immunity protein, included size, isoelectric point, predicted subcellular localization, and the presence of a cysteine-histidine catalytic dyad.

In this study, we performed an informatic search for T6SS substrates and found previously unidentified families of peptidoglycan glycoside hydrolase effectors, herein named Tge proteins (type VI secretion glycoside hydrolase effectors). Characterization of a representative Tge from *P. protegens* showed that the protein displays periplasmic toxicity, is secreted in a T6-dependent manner, and confers a fitness advantage when *P. protegens* is grown in competition against *P. putida*, a co-occurring soil bacterium. Additionally, we solved the 1.4 Å crystal structure of *P. protegens* Tge in complex with its cognate immunity protein. Together, our findings show a broader distribution of T6S glycoside hydrolase effectors than was previously appreciated and offer insights into the molecular basis for glycoside hydrolase activity and inhibition.

EXPERIMENTAL PROCEDURES

Bioinformatic Screen—Putative effector-immunity candidates were identified using a similar informatic search protocol as described previously (9). Briefly, a custom Perl script was used to search 115 T6SS$^+$ genomes for bicistronic genes with the following criteria for the encoded effector protein: 1) no predicted signal sequence, 2) a predicted pI greater than 8.0, and 3) fewer than 200 amino acids. The criteria for the immunity protein included the presence of a predicted signal sequence and fewer than 200 amino acids. Protein sequences obtained from this screen were submitted in batch mode to the Phyre^2 server and examined manually for the presence of lysozyme-like folds (19). Candidate peptidoglycan glycoside hydrolases and associated immunity proteins were then used as Blastp search queries to identify all unique family members in the NCBI database.

Bacterial Strains and Growth Conditions—All *P. protegens* strains generated in this study were derived from the sequenced strain Pf-5 (20). *P. protegens* strains were grown in Luria-Bertani (LB) media at 30 °C supplemented with 15 μg ml^{-1} gentamycin and 25 μg ml^{-1} irgasan where appropriate. The pEXG2 suicide vector was used for in-frame chromosomal deletions in *P. protegens* as described previously for *P. aeruginosa* (21). Similar to *P. aeruginosa*, deletion of *retS* is required for activation of T6S in *P. protegens* (22, 23). Locus tags for *retS*, *tge2^{PP}*, *tgi2^{PP}*, and *clpV* are PFL_0664, PFL_3037, PFL_3036, and PFL_6093, respectively. The *P. putida* strain used for competition assays was derived from the sequenced strain KT2440 (24) and grown in LB media at 30 °C. *E. coli* strains used included DH5α for cloning, SM10 for conjugal transfer of plasmids into *P. protegens*, BL21 pLysS for toxicity assays, growth curves, and phase contrast microscopy, and Shuffle® T7 Express *lysY* (New England Biolabs) for expression of proteins for purification. *E. coli* strains were either grown in LB or LB low salt (LB-LS) at 37 °C supplemented with 50 μg ml^{-1} kanamycin, 150 μg ml^{-1} carbenicillin, 30 μg ml^{-1} chloramphenicol, 200 μg ml^{-1} trimethoprim, 0.1% (w/v) L-rhamnose and the indicated concentrations of IPTG as required.

E. coli Toxicity Assays—*Tge2^{PP}* was cloned into pET-29b(+) and pET-22b(+) using the BamHI/HindIII and NdeI/HindIII restriction sites, respectively. *Tgi2^{PP}* and *tgi1^{PA}* (PA3485) were cloned into pSCrhaB2-CV using the NdeI/XbaI restriction sites. The *tge2^{PP}* E69Q mutation was introduced using SOE

PCR. Overnight cultures of *E. coli* BL21 pLysS pET-29b(+), pET-29b(+)::*tge2*^{PP}, pET-22b(+), pET-22b(+)::*tge2*^{PP}, pET-22b(+)::*tge2*^{PP} E69Q, pET-22b(+) + pSCrhaB2-CV, pET-22b(+)::*tge2*^{PP} + pSCrhaB2-CV, pET-22b(+)::*tge2*^{PP} + pSCrhaB2-CV::*tgi2*^{PP} and pET-22b(+)::*tge2*^{PP} + pSCrhaB2-CV::*tgi1*^{PA} were diluted 10^6 in 10-fold increments and stamp plated onto LB-LS 3% agar plates containing the appropriate antibiotics. For comparison of cytoplasmic *versus* periplasmic toxicity of Tge2^{PP}, cells were induced with 100 μM IPTG. For immunity rescue experiments, expression was induced with 40 μM IPTG for Tge2^{PP} and 0.1% (w/v) L-rhamnose for Tgi2^{PP}/Tgi1^{PA}. Western blot analysis of Tge2^{PP} and Tge2^{PP} E69Q expression levels was performed using an anti-His HRP conjugate according to the manufacturer's instructions (Qiagen). The *E. coli* BL21 pLysS expression strain was used in these experiments to prevent leaky expression prior to IPTG induction.

Interbacterial Competitions—Competition experiments were performed in a similar manner as described previously for *B. thailandensis* (9). Briefly, *P. protegens* and *P. putida* strains were mixed in a 1:1 ratio, and 10 μl of the mixture was spotted on 0.2-μm nitrocellulose membrane overlaid on LB-LS 3% agar plates. Plate counts were taken of the initial innoculum and after 18 h of competition at 30 °C. The recipient *P. putida* strain contained a GFP expression construct integrated into the attTn7 site allowing for differentiation of the donor and recipient cells using fluorescence imaging as described previously (1, 25, 26). Statistical analyses were carried out using a two-tailed Student's *t* test.

P. protegens Secretion Assay and Western Blot Analysis—*Tge2*^{PP}, including its native ribosome binding site, were cloned into pPSV35-CV using the SacI/XbaI restriction sites. The resulting construct encodes Tge2^{PP} fused to a C-terminal vesicular stomatitis virus G (VSV-G) epitope tag to facilitate detection by immunoblotting. Overnight cultures of *P. protegens* Δ*retS* and Δ*retS* Δ*clpV* harboring pPSV35-CV::*tge2*^{PP} were subcultured 1:500 into LB containing 100 μM IPTG and grown to mid-log phase. Cell and supernatant fractions were separated and analyzed for the presence of Tge2^{PP} by Western blot using an anti-VSV-G antibody as described previously (21).

Growth Curves—Overnight cultures of *E. coli* BL21 pLysS containing pET-22b(+), pET-22b(+)::*tge2*^{PP} and pET-22b(+)::*tge2*^{PP} E69Q were subinoculated to an optical density at 600 nm (A_{600}) of 0.01 in LB-LS and grown at 37 °C. A_{600} measurements were taken every 30 min until the cultures reached an A_{600} of ~0.2, at which point protein expression was induced with 100 μM IPTG. Following IPTG induction, A_{600} measurements were taken every 15 min for the remainder of the growth curve.

Protein Expression and Purification—For the isothermal titration calorimetry (ITC) experiment, full-length *tge2*^{PP} and *tgi2*^{PP} lacking its encoded signal sequence (Tgi2^{PP}(24–156) were cloned into pET-28b(+) and pET-15b using the NdeI/XhoI and NdeI/BamHI restriction sites, respectively, to generate N-terminal His_6 tags on both proteins. For crystallization, full-length *tge2*^{PP} was cloned into pET-24a(+) using the NdeI/XhoI restriction sites to generate an untagged construct suitable for coexpression with the Tgi2^{PP}(24–156) construct described above. All protein constructs were expressed in Shuffle® T7 Express *lysY* cells, which allow for cytoplasmic disulfide bond formation, and grown in LB broth supplemented with the appropriate antibiotics. For each construct, cells were grown at 37 °C to an A_{600} of 0.6 before protein expression was induced with 1 mM IPTG at room temperature for 18 h. For the protein samples used in the ITC experiment, cells were resuspended in 50 mM sodium phosphate, pH 7.2, 300 mM NaCl, 5 mM imidazole, and lysed by sonication. Following centrifugation, the cleared cell lysates were purified by Ni^{2+}-nitrilotriacetic acid affinity chromatography using a linear gradient of 5–400 mM imidazole. The purified proteins were then dialyzed against 20 mM sodium phosphate, pH 7.2, 150 mM NaCl prior to use in downstream experiments. For crystallization, cells containing coexpressed Tge2^{PP}/Tgi2^{PP}(24–156) were resuspended in 50 mM Hepes, pH 7.5, 300 mM NaCl, 5 mM imidazole, and lysed by sonication. The complex was then purified using Ni^{2+}-nitrilotriacetic acid affinity chromatography in 20 mM Hepes, pH 7.5, 300 mM NaCl, 5–400 mM imidazole followed by size exclusion chromatography in 20 mM Hepes, pH 7.5, 150 mM NaCl.

Isothermal Titration Calorimetry—Purified Tge2^{PP} and Tgi2^{PP}(24–156) were degassed before experimentation. ITC measurements were performed with a VP-ITC microcalorimeter (MicroCal Inc., Northampton, MA). Titrations were carried out with 250 μM Tgi2^{PP}(24–156) in the syringe and 16 μM Tge2^{PP} in the cell. The titration experiment consisted of one 2-μl injection followed by 29 5-μl injections with 300-s intervals between each injection. The ITC data were analyzed using the Origin software (version 5.0, MicroCal, Inc.) and fit using a single-site binding model.

Phase Contrast Microscopy—Phase contrast microscopy images were acquired with a Nikon Ti-E inverted microscope fitted with a 60× oil objective, a xenon light source (Sutter Instruments), and a CCD camera (Clara series, Andor). Overnight cultures of *E. coli* BL21 pLysS pET-22b(+)::*tge2*^{PP} and pET-22b(+)::*tge2*^{PP} E69Q were subcultured 1:300 into LB broth containing the appropriate antibiotics and grown to an A_{600} of 0.2. IPTG was then added to a concentration of 200 μM, and after a 45-min incubation, the bacterial suspension (1 μl) was spotted onto growth pads made with LB-LS medium and 1% (*w/v*) agarose, and cells were imaged immediately.

Crystallization and Structure Determination—Selenomethionyl-incorporated Tge2^{PP}·Tgi2^{PP}(24–156) complex was concentrated to 10 mg ml^{-1} by spin ultrafiltration (10 kDa molecular mass cut-off, Millipore) and screened against commercially available sparse matrix crystal screens (Crystal Screens 1 and 2, Hampton Research). Crystal trials were setup in 48-well plates using the sitting drop vapor diffusion technique. Protein and crystallization solutions were mixed in a 1:1 ratio with a final drop size of 2 μl suspended over 250 μl of crystallization solution and stored at room temperature.

After 3–4 days, diffraction quality crystals grew in 0.1 M Tris-HCl, pH 8.5, 0.2 M $CaCl_2$, and 30% (w/v) PEG 4000 and were flash frozen without any added cryoprotectant. X-ray diffraction data were collected on beamline 5.0.3 at the Lawrence Berkeley National Laboratory Advanced Light Source (27). The data were merged, integrated, and scaled using the *xia2* system (28). Experimental phases were obtained using the Phenix AutoSol Wizard (29) resulting in density modified selenium single-wavelength anomalous diffraction phased maps of

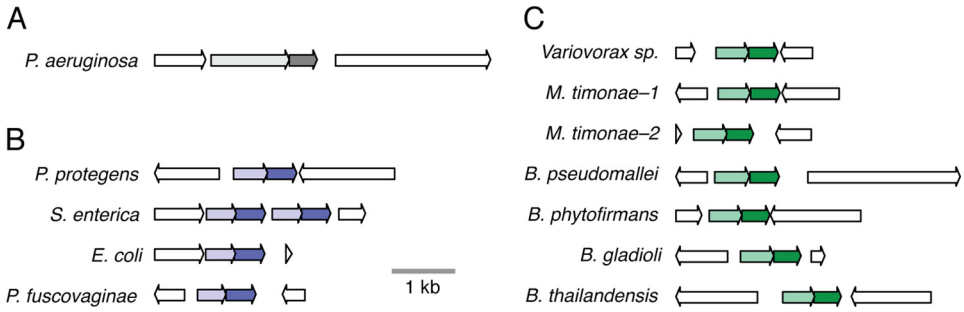

FIGURE 1. **Overview of the *tge1–3* families.** Genomic arrangement of *tge1* (*A*), *tge2* (*B*), and *tge3* (*C*) families in representative organisms. Shading is used to indicate effector (*light*) and immunity (*dark*) open reading frames. Accession numbers and sequence alignments of Tge2 and Tge3 effector and immunity proteins are available in supplemental Figs. S1 and S2.

excellent quality, which allowed for automated model building with the Phenix AutoBuild Wizard (30). Subsequent model adjustments were made manually in COOT (31) between iterative rounds of refinement carried out using PHENIX.REFINE (32). The final model was refined to an R_{work}/R_{free} of 14.9% and 17.5% (Table 1).

RESULTS

Identification of Peptidoglycan Glycoside Hydrolase Effector/Immunity Families—Previously, we reported the development of a heuristic search method that was successfully employed for the identification of a widespread type VI peptidoglycan amidase effector superfamily (9). Using a customized Perl script, T6SS$^+$ genomes were searched for bicistrons that encode protein products with a defined set of properties commonly associated with T6S effector-immunity pairs. For the effector protein, this included the absence of a signal peptide, an isoelectric point greater than 8.0, fewer than 200 amino acids, and the presence of conserved catalytic histidine and cysteine residues. Parameters used for the immunity protein included the presence of a signal peptide and primary sequence length limitation (<200 amino acids). These selection criteria yielded 418 total candidate E-I pairs, within which amidase effectors were identified by structure prediction algorithms and subsequent direct experimentation (19). To adapt this pipeline for the identification of glycoside hydrolase effectors, we excluded the histidine and cysteine constraints, generating a list of 831 candidate E-I pairs from 115 T6SS$^+$ genomes. These were then examined by structure prediction servers to identify lysozyme-like folds and manually curated to remove systematic false-positives (see "Experimental Procedures"). This approach yielded two phylogenetically distinct families, which combine with *P. aeruginosa* Tse3 to form the basis for three distinct type VI peptidoglycan glycoside hydrolase effector and immunity groups (Tge1–3 and Tgi1–3) (Fig. 1 and supplemental Figs. S1 and S2). Although it likely functions as a muramidase, we have opted not to include *V. cholerae* VgrG-3 in this reclassification of T6S glycoside hydrolase effectors. This emphasizes the additional postulated structural role of VgrG-3 in the T6S apparatus, which has not been observed for non-VgrG-fused effectors similar to the Tge1–3 proteins (11, 16).

Many peptidoglycan glycoside hydrolases share a lysozyme-like fold; however, they can be divided into two enzymatic subgroups based on their cleavage mechanism. Lysozymes and lytic transglycosylases cleave the β-1,4-glycosidic bond between MurNAc and GlcNAc, the former hydrolyzing the bond forming a reducing MurNAc end, and the latter catalyzing the formation of 1,6-anhydroMurNAc (33). In contrast, *N*-acetylglucosaminidases cleave the β-1,4-glycosidic bond between GlcNAc and MurNAc, leaving GlcNAc as the reducing sugar. Irrespective of their substrate specificity, peptidoglycan glycoside hydrolases universally employ a conserved glutamate, acting as a catalytic acid, to initiate cleavage of the glycosidic bond (33). Consistent with our hypothesis that Tge2 and Tge3 proteins such as Tse3 function as peptidoglycan glycoside hydrolase enzymes, we identified a strictly conserved Glu within a putative active motif in both enzyme families (supplemental Figs. S1 and S2). Additionally, our sequence analyses indicated that Tge2 proteins likely hydrolyze peptidoglycan using a standard goose-type (G-type) single displacement mechanism (34), whereas the Tge3 family contains a Glu-Asp-Thr catalytic triad utilized by phage-type lysozymes (35, 36).

Tge2^{PP}-Tgi2^{PP} Are an Effector-immunity Pair Secreted by the T6SS—Tge1 from *P. aeruginosa* (Tge1^{PA}, formerly Tse3) has been demonstrated previously to function as a peptidoglycan glycoside hydrolase effector. To validate a new family identified by our informatics search, we chose to characterize a Tge2-Tgi2 E-I pair from the soil-dwelling bacterium *P. protegens* (Tge2^{PP}-Tgi2^{PP}). To confirm that Tge2^{PP} functions as a periplasmic effector, we performed toxicity assays in *E. coli*. As expected for a peptidoglycan-degrading enzyme, we observed a significant decrease in *E. coli* viability and optical density when Tge2^{PP} was artificially targeted to the periplasm via a *sec*-dependent leader sequence (peri-Tge2^{PP}, Fig. 2, *A* and *B*). Furthermore, these effects of Tge2^{PP} periplasmic toxicity were specific to Tge2^{PP} catalytic activity, as a conservative mutation of its predicted catalytic glutamate (E69Q) abolished toxicity. Consistent with its proposed role as a peptidoglycan glycoside hydrolase effector, peri-Tge2^{PP} induced cell rounding and lysis compared with the catalytic point mutant (Fig. 2*C*). Importantly, Western blot analysis confirmed that the observed reduction in toxicity and cell rounding was not due to decreased expression levels of the E69Q protein relative to wild-type (Fig. 2*D*). Despite our ability to observe Tge2^{PP} activity in a cellular context, we were unable to detect significant degradation of purified peptidoglycan sacculi by Tge2^{PP} over a range of conditions, raising the intriguing

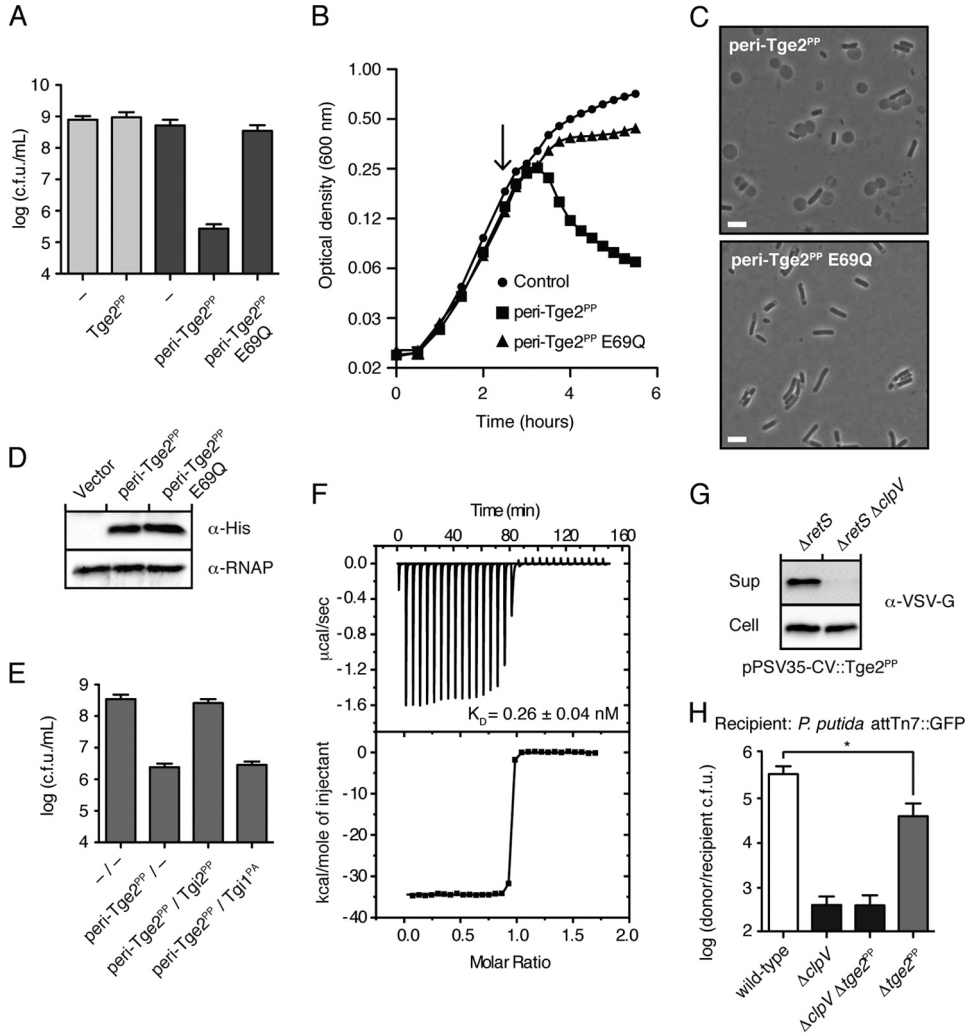

FIGURE 2. **Tge2^{PP}-Tgi2^{PP} are an effector-immunity pair secreted by the T6SS.** *A*, growth of *E. coli* on solid media harboring inducible plasmids expressing the indicated proteins. Empty vector controls are indicated by a *dash*. *Error bars* represent ± S.D. ($n = 3$). *B*, optical density of *E. coli* in liquid media harboring a vector control or inducible plasmids expressing the indicated proteins. The *arrow* indicates the time at which protein expression was induced. *Error bars* represent ± S.D. ($n = 3$). *C*, representative phase contrast micrographs of *E. coli* expressing peri-Tge2^{PP} or peri-Tge2^{PP} E69Q. Images were acquired 45 min after IPTG induction. *Scale bar*, 2 μm. *D*, Western blot analysis of *E. coli* expressing vector control, Tge2^{PP} and Tge2^{PP} E69Q. RNA polymerase (*RNAP*) was used as a loading control. *E*, growth of *E. coli* on solid media harboring inducible plasmids expressing the indicated proteins. Empty vector controls are indicated by a *dash*. *Error bars* represent ± S.D. ($n = 3$). *F*, ITC analysis showing the interaction between Tge2^{PP} and Tgi2^{PP}. The *top panel* displays the heats of injection, whereas the *bottom panel* shows the normalized integration data as a function of the molar syringe and cell concentrations. *G*, Tge2^{PP} is secreted in a T6-dependent manner. Western blot analysis of the cell and supernatant (*sup*) fractions of the indicated *P. protegens* strains expressing Tge2^{PP} fused to a C-terminal vesicular stomatitis viral glycoprotein (*VSV-G*) tag. *H*, Tge2^{PP} provides a competitive growth advantage under cell contact-promoting conditions. Competitive outcome of the indicated *P. protegens* strains against *P. putida*. *Asterisks* denote competition outcomes significantly different than wild-type *P. protegens* ($n = 4$; *, $p < 0.05$). *Error bars* indicate ± S.D.

possibility that the effector may require a yet unidentified periplasmic cofactor or binding partner.

Next, we examined whether Tgi2^{PP} could inhibit the toxicity exhibited by peri-Tge2^{PP}. Tgi2^{PP} co-expressed with peri-Tge2^{PP} significantly rescued Tge2^{PP}-dependent toxicity, indicating that Tgi2^{PP} functions as an immunity protein (Fig. 2*E*). As predicted by its lack of sequence homology to Tgi2^{PP}, co-expression of *P. aeruginosa* Tgi1 (Tgi1^{PA}, formerly Tsi3) was not able to rescue *E. coli* viability. Next, we investigated the mechanism of inhibition of Tge2^{PP} activity by Tgi2^{PP}. To probe for a direct binding mechanism, we conducted ITC measurements on purified Tge2^{PP} and Tgi2^{PP}. The binding isotherm obtained by titration of the effector with Tgi2^{PP} fit a single-site binding model with a stoichiometry of ~1:1 ($n = 0.93$) and a dissociation constant of 0.26 ± 0.04 nM (Fig. 2*F*). Titration of Tgi2^{PP} into buffer and buffer into Tge2^{PP} confirmed that the observed saturation of the heats of injection was due to the Tge2^{PP}-Tgi2^{PP} interaction and not between either of the proteins and a component of the buffer solution (supplemental Fig. S3). The tight binding observed between Tge2^{PP} and Tgi2^{PP} is consistent with the affinities measured for other T6SS E-I pairs, including *P. aeruginosa* Tae1-Tai1, *Enterobacter cloacae* Tae4-Tai4, and two Tae4-Tai4 family members from *S. marcescens*, which all bind with low nanomolar to high picomolar dissociation constants (12, 13, 15).

P. aeruginosa possesses three functionally non-redundant T6SSs, encoded by HSI-I-III. Of these, the H1-encoded system is post-transcriptionally activated by the Gac/Rsm pathway (23). *P. protegens* possesses only a single T6SS. This system is orthologous to the H1-T6SS, and is also regulated by the Gac/

TABLE 1
X-ray data collection and refinement statistics

	$Tge2^{PP}/Tgi2^{PP}$
Data collection	
Beamline	ALS 5.0.3
Wavelength (Å)	0.976
Space group	$P2_12_12_1$
Cell dimensions	a = 40.1, b = 81.5, and c = 86.4 Å; α = 90.0, β = 90.0, and γ=90.0°
Resolution (Å)	59.31–1.44 (1.47–1.44)[a]
Total no. of reflections	348,034
Total no. of unique reflections	52,547
R_{sym} (%)[b]	5.7 (53.0)[a]
$I/\sigma I$	15.1 (2.2)[a]
Completeness (%)	99.9 (99.9)[a]
Redundancy	6.6 (4.6)[a]
Refinement	
R_{work}/R_{free} (%)[c]	14.9/17.5
No. of atoms	
Protein	2005
Water	353
Average B-factors (Å^2)	
Protein	21.3
Water	32.7
r.m.s.d.[d]	
Bond lengths (Å)	0.007
Bond angles	1.105°
Ramachandran plot (%)[e]	
Total favored	98.1
Total allowed	100.0
Coordinate error (Å)[f]	0.13

[a] Values in parentheses correspond to the highest resolution shell.
[b] $R_{sym} = \Sigma\Sigma|I(k) - \langle I\rangle|/\Sigma I(k)$ where $I(k)$ and $\langle I\rangle$ represent the diffraction intensity values of the individual measurements and the corresponding mean values. The summation is over all unique measurements.
[c] $R_{work} = \Sigma||F_{obs}| - k|F_{calc}||/|F_{obs}|$ where F_{obs} and F_{calc} are the observed and calculated structure factors, respectively. R_{free} is the sum extended over a subset of reflections (5%) excluded from all stages of the refinement.
[d] r.m.s.d. indicates root mean square deviation.
[e] Values were calculated using MOLPROBITY (52).
[f] Shown is the maximum likelihood-based coordinate error, as determined by PHENIX (53).

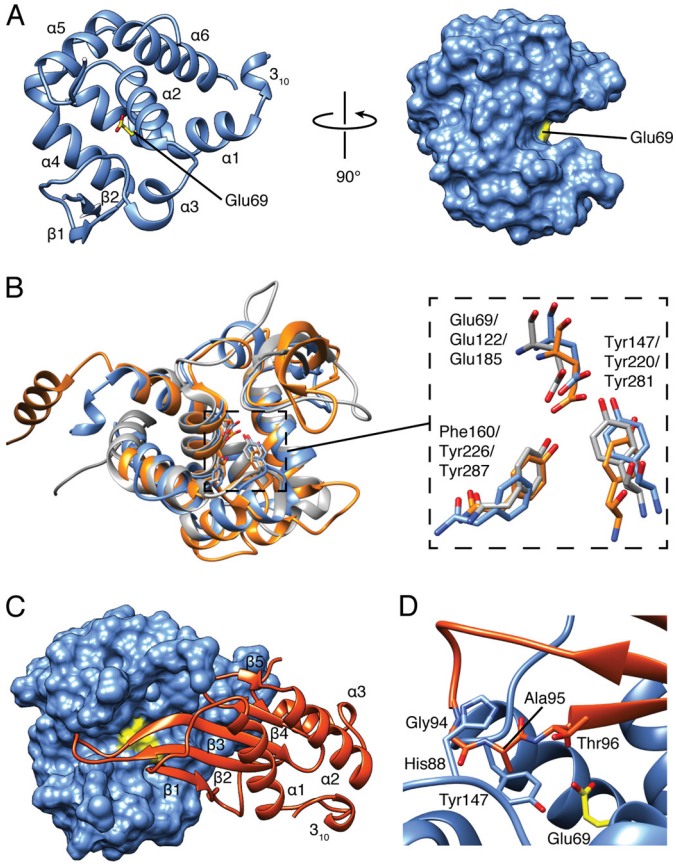

FIGURE 3. **Overall structure of $Tge2^{PP}$ in complex with $Tgi2^{PP}$.** *A*, $Tge2^{PP}$ adopts a lysozyme-like fold. Ribbon (*left*) and surface (*right*) representations of $Tge2^{PP}$ shown at two orthogonal orientations. Secondary structure elements and the catalytic acid, Glu^{69}, are labeled. $Tgi2^{PP}$ is omitted for clarity. *B*, structural overlay of $Tge2^{PP}$ (*blue*), Auto (*orange*), and FlgJ (*gray*) shown as schematic representations (*left panel*). Superposition of the $Tge2^{PP}$, Auto and FlgJ active site residues are shown as stick representations (*right panel*). The labels indicate the residue numbering of $Tge2^{PP}$ followed by Auto and FlgJ. *C*, structure of the $Tge2^{PP}$·$Tgi2^{PP}$ complex. $Tge2^{PP}$ and $Tgi2^{PP}$ are shown as surface and ribbon representations, respectively. Secondary structure elements of $Tgi2^{PP}$ are labeled, and Glu^{69} of $Tge2^{PP}$ is colored *yellow*. *D*, a protruding loop of $Tgi2^{PP}$ occludes the active site of $Tge2^{PP}$. Shown is a close-up view of the $\beta2$-$\beta3$ loop of $Tgi2^{PP}$ interacting with the active site of $Tge2^{PP}$. Invariant residues Gly^{94} and Ala^{95} of $Tgi2^{PP}$ interact with His^{88} and Tyr^{147} in the active site cleft of $Tge2^{PP}$.

Rsm pathway (22). The RetS hybrid sensor kinase functions within the Gac/Rsm pathway as a negative regulator of T6S (2, 22, 23). Given that T6SSs are largely quiescent under *in vitro* cultivation conditions, we used a *P. protegens* Δ*retS* strain to test the hypothesis that $Tge2^{PP}$ is a T6SS substrate. Robust secretion of $Tge2^{PP}$ was observed in the supernatant fraction of the parental strain; however, this was abrogated in a *P. protegens* strain containing the additional deletion of the gene encoding the essential type VI component, ClpV (Fig. 2*G*). Given that $Tge2^{PP}$ is secreted by the T6SS, we next sought to ascertain its contribution to interbacterial fitness. When *P. protegens* strains were competed under cell contact-promoting conditions against *P. putida*, a bacterium that inhabits similar environments (37, 38), those lacking $tge2^{PP}$ were ~6-fold less fit compared with the wild-type (Fig. 2*H*). Although this difference is highly significant and confirms the role of $Tge2^{PP}$ as a T6 effector, it is also interesting to note that *P. protegens* strains with a non-functional T6SS display a ~1000-fold decrease in competitive fitness against *P. putida*. This finding suggests that there are other currently uncharacterized effectors produced by *P. protegens* that mediate antagonistic interactions between these organisms. In total, these data indicate that $Tge2^{PP}$ is an antibacterial T6S effector.

Structure of the $Tge2^{PP}$·$Tgi2^{PP}$ Complex—To gain further insight into $Tge2^{PP}$ function and its mode of inhibition by $Tgi2^{PP}$, we determined the 1.4 Å crystal structure of the $Tge2^{PP}$·$Tgi2^{PP}$ complex using the single-wavelength anomalous diffraction technique with selenomethionyl-incorporated protein (Table 1). Crystals of the $Tge2^{PP}$·$Tgi2^{PP}$ complex grew in the orthorhombic space group $P2_12_12_1$ and contained a single 1:1 complex in the asymmetric unit. Disordered residues not built in the final model include 1–29, 101–104, and 152–155 of $Tge2^{PP}$, and residues 24–26, 155–156, and the N-terminal His_6 tag of $Tgi2^{PP}$. The final model was refined to an R_{work} and R_{free} of 14.9% and 17.5%, respectively.

$Tge2^{PP}$ Resembles Family 73 Glycoside Hydrolases—$Tge2^{PP}$ adopts a lysozyme-like fold consisting of large and small lobes that are positioned such that a substrate-binding groove is formed between them (Fig. 3*A*). The large lobe is made up of a short 3_{10} helix, $\alpha1$-$\alpha2$ and $\alpha4$-$\alpha6$, whereas the small lobe consists of $\alpha3$ and a β-hairpin formed by $\beta1$-$\beta2$. The termini are covalently linked by a Cys^{32}-Cys^{177} disulfide bond, which connects the N-terminal 3_{10} helix to the C-terminal loop. As determined by DALI (39), the overall structure resembles closely that of glycoside hydrolase family 73 members, which includes the

peptidoglycan hydrolase FlgJ from *Sphingomonas* sp. strain A1 (Z-score, 16.4; C_α root mean square deviation of 1.6 Å over 124 equivalent positions) and Auto, a peptidoglycan *N*-acetylglucosaminidase from *Listeria monocytogenes* (Z-score, 13.9; C_α root mean square deviation of 2.6 Å over 126 equivalent positions) (Fig. 3*B*) (40, 41). It is proposed that members of this family catalyze the hydrolysis of peptidoglycan using a single displacement mechanism similar to that originally demonstrated for G-type egg white lysozyme (GEWL). In this mechanism, a catalytic glutamate donates a proton to the scissile glycosidic bond, resulting in its cleavage and formation of an oxocarbenium intermediate. This short-lived intermediate then undergoes nucleophilic attack by a water molecule, resulting in the hydrolyzed product with inverted stereochemistry at the anomeric position (34). In agreement with our functional studies, the catalytic glutamate in $Tge2^{PP}$ corresponds to Glu^{69}, inferred from its nearly identical position to the corresponding glutamate residue in both FlgJ and Auto (Fig. 3*B*). Glu^{69} protrudes from the end of α2 and lies deep within the substrate-binding groove. In addition, the hydroxyl group of Tyr^{147} forms a hydrogen bond with Glu^{69}, in a manner similar to the aforementioned peptidoglycan glucosaminidase and G-type lysozyme enzymes, perhaps to orient it for catalysis.

$Tgi2^{PP}$ Inhibits $Tge2^{PP}$ by Protruding into the Substrate-binding Groove—The structure of $Tgi2^{PP}$ consists of a short N-terminal 3_{10} helix and a central five-stranded β-sheet flanked by three α-helices (Fig. 3*C*). A Cys^{117}-Cys^{152} disulfide bond connects β5 to the C-terminal loop, anchoring α3 to the β-sheet core. $Tgi2^{PP}$ does not share strong structural similarity to other proteins of known structure; however, it does contain a similar topology to the periplasmic *E. coli* colicin M immunity protein (Z-score, 3.5; C_α root mean square deviation of 3.7 Å over 62 equivalent positions) (42). Colicin M is a bacteriocin with phosphatase activity that targets the undecaprenyl phosphate-linked peptidoglycan precursors lipid I and lipid II in the periplasm of recipient bacteria (43). The observation that the colicin M immunity protein resembles $Tgi2^{PP}$ suggests that these immunity proteins may have undergone diversifying selection to acquire effector specificity.

The interaction between $Tge2^{PP}$ and $Tgi2^{PP}$ involves the insertion of the β-sheet core of $Tgi2^{PP}$ into the substrate-binding groove of $Tge2^{PP}$. Most notably, the elongated loop connecting β2 and β3 protrudes into the active site in an orientation predicted to prevent the catalytic glutamate from accessing its peptidoglycan substrate. Overall, the $Tge2^{PP}$·$Tgi2^{PP}$ complex consists of a 1237 $Å^2$ interface stabilized predominantly by hydrogen bonding and hydrophobic interactions. Conservation mapping of $Tgi2^{PP}$ homologs suggests that invariant residues Gly^{94} and Ala^{95}, which are located in the β2-β3 loop, are important for direct interaction with the active site of $Tge2^{PP}$ (Fig. 3*D*). Binding site analysis using PDBePISA indicates that the amide nitrogen and oxygen atoms of Gly^{94} form hydrogen bonding interactions with the main chain of Tyr^{147} and His^{88} of $Tge2^{PP}$, respectively, whereas the side chain of Ala^{95} becomes desolvated upon complex formation (44). Additional conserved interfacing residues include Tyr^{56}, Asp^{66}, Leu^{69}, His^{78}, Tyr^{88}, Pro^{91}, Trp^{99}, Gly^{100}, Leu^{101}, Glu^{113}, Cys^{117}, Gly^{149}, Leu^{150}, Gly^{151}, Cys^{152}, and Asp^{154}. The inhibition mode observed in the $Tge2^{PP}$·$Tgi2^{PP}$ complex is reminiscent of bacterial proteinaceous inhibitors of eukaryotic lysozymes. The *E. coli* inhibitor of vertebrate lysozyme (Ivy), *P. aeruginosa* membrane-bound lysozyme inhibitor of C-type lysozyme (MliC), and *E. coli* PliG (periplasmic lysozyme inhibitor of G-type lysozyme) all use active site occlusion as a mechanism of inhibition (Fig. 4) (45–47). Moreover, in each case, the region involved in inhibition consists of a loop region connecting two β-strands. However, it is interesting to note that there is little fold similarity between these lysozyme inhibitors, suggesting they arose through convergent evolution.

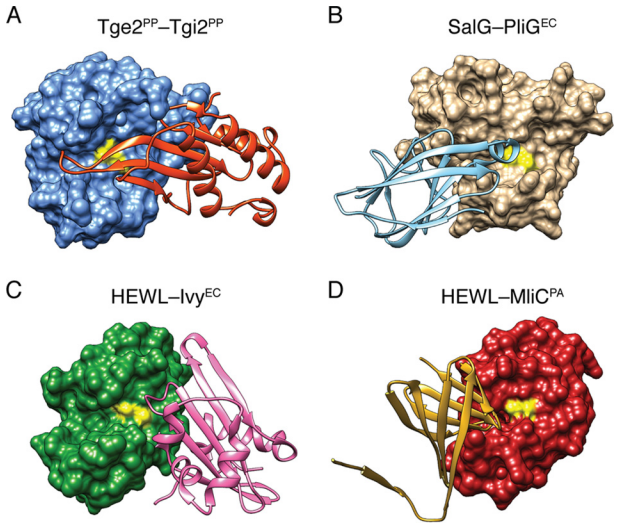

FIGURE 4. **Structurally characterized lysozyme inhibitors display distinct folds but act via a common mechanism.** Comparison of the $Tge2^{PP}$·$Tgi2^{PP}$ complex to vertebrate lysozymes in complex with proteinaceous bacterial lysozyme inhibitors. Shown are the $Tge2^{PP}$·$Tgi2^{PP}$ complex (*A*), *E. coli* periplasmic lysozyme inhibitor of G-type lysozyme ($PliG^{EC}$) in complex with salmon G-type lysozyme (*SalG*) (*B*), *E. coli* proteinaceous inhibitor of vertebrate lysozyme (Ivy^{EC}) in complex with hen egg white lysozyme (*HEWL*) (*C*), and membrane-bound lysozyme inhibitor of C-type lysozyme (MliC) in complex with hen egg white lysozyme (*D*) (45–47). For each structural model, the lysozyme-like protein and its associated inhibitor are shown as surface and ribbon representations, respectively.

DISCUSSION

In this work, we identified two families of T6S peptidoglycan glycoside hydrolase effectors using informatic methods. Previously, we used homology-independent search criteria to identify a T6S peptidoglycan amidase effector superfamily. The identification of the peptidoglycan glycosyl hydrolase families described herein further exemplifies the utility of this method as a means to identify novel effector-immunity pairs. Prior characterization of $Tge1^{PA}$ has shown that this enzyme possesses β-(1,4)-*N*-acetylmuramidase (lysozyme) activity. Furthermore, $Tge1^{PA}$ contains a GL*X*Q motif found in both GEWL and *E. coli* soluble lytic transglycosylase (Slt70) in addition to its catalytic glutamate, suggesting it is likely structurally similar to these enzymes (3, 48). Interestingly, Tge3 family members contain a conserved Glu-Asp-Thr catalytic triad reminiscent of phage T4 lysozyme. Thus, similar to Tge1, we expect this family to exhibit β-(1,4)-*N*-acetylmuramidase activity. In contrast, we find that $Tge2^{PP}$ most closely resembles members of a peptidoglycan hydrolase family with ascribed *N*-acetylglucosaminidase activity. Members of this family contain a catalytic glutamate residue embedded in an AA*X*E(S/T) motif.

This observation suggests that Tge2 enzymes could target a different chemical bond in the peptidoglycan backbone to facilitate breakdown of the cell wall in recipient bacteria.

Bacteria are known to chemically modify the glycan moieties of peptidoglycan. As this can affect their susceptibility to cell wall-targeting enzymes, it is intriguing to speculate that the different peptidoglycan glycoside hydrolase effectors delivered by the T6SS could harbor specificity for the presence or absence of these modifications. Modifications influencing muramidase activity include MurNAc and GlcNAc de-*N*-acetylation, as well as MurNAc *O*-acetylation (49). These generally result in lysozyme resistance, whereas *N*-acetylglucosaminidase enzymes can be unaffected by the acetylation state of peptidoglycan (50). Future studies will be needed to address the specificity of the Tge families, as well as the extent to which particular cell wall modifications influence their activity.

In light of the peptidoglycan glycoside hydrolases identified in this study, it is now apparent *P. aeruginosa* is not the only bacterium that secretes multiple T6 effectors targeting peptidoglycan. For example, in addition to Tge2 peptidoglycan glycoside hydrolases, *Salmonella* Typhi and *P. protegens* also possess Tae2 and Tae3 peptidoglycan amidases, respectively (9). The reason for secreting a multitude of peptidoglycan-targeting T6S effectors may be myriad. It is conceivable that the T6 donor bacterium requires complete digestion of recipient peptidoglycan sacculi to utilize it as a carbon source after lysis occurs. A non-mutually exclusive explanation may be the existence of enzymatic synergy between amidase and muramidase effectors, wherein the breakdown product of one enzyme may make the substrate of the second more accessible. The importance of this type of enzymatic synergy was recently demonstrated for cellulose-degrading enzymes (51). Alternatively, the various E-I loci within a given organism may be subject to differential regulation, such that the effector most beneficial in a particular environmental condition is expressed. The magnitude of this disproportionate benefit could be dependent upon the target organism(s) present, the physiological state of the target(s) (*e.g.* growing *versus* sessile), and the osmolarity of the surrounding milieu.

Acknowledgments—We thank Dr. P. Lynne Howell at the Hospital for Sick Children (Toronto, Canada) for providing reagents and laboratory equipment during the early stages of this work, Dr. William Catterall for use of the ITC instrument, and Michele LeRoux for microscopy expertise.

REFERENCES

1. Schwarz, S., West, T. E., Boyer, F., Chiang, W. C., Carl, M. A., Hood, R. D., Rohmer, L., Tolker-Nielsen, T., Skerrett, S. J., and Mougous, J. D. (2010) Burkholderia type VI secretion systems have distinct roles in eukaryotic and bacterial cell interactions. *PLoS Pathog.* **6,** e1001068
2. Hood, R. D., Singh, P., Hsu, F., Güvener, T., Carl, M. A., Trinidad, R. R., Silverman, J. M., Ohlson, B. B., Hicks, K. G., Plemel, R. L., Li, M., Schwarz, S., Wang, W. Y., Merz, A. J., Goodlett, D. R., and Mougous, J. D. (2010) A type VI secretion system of *Pseudomonas aeruginosa* targets a toxin to bacteria. *Cell Host Microbe* **7,** 25–37
3. Russell, A. B., Hood, R. D., Bui, N. K., LeRoux, M., Vollmer, W., and Mougous, J. D. (2011) Type VI secretion delivers bacteriolytic effectors to target cells. *Nature* **475,** 343–347
4. Leiman, P. G., Basler, M., Ramagopal, U. A., Bonanno, J. B., Sauder, J. M., Pukatzki, S., Burley, S. K., Almo, S. C., and Mekalanos, J. J. (2009) Type VI secretion apparatus and phage tail-associated protein complexes share a common evolutionary origin. *Proc. Natl. Acad. Sci. U.S.A.* **106,** 4154–4159
5. Pell, L. G., Kanelis, V., Donaldson, L. W., Howell, P. L., and Davidson, A. R. (2009) The phage λ major tail protein structure reveals a common evolution for long-tailed phages and the type VI bacterial secretion system. *Proc. Natl. Acad. Sci. U.S.A.* **106,** 4160–4165
6. Koskiniemi, S., Lamoureux, J. G., Nikolakakis, K. C., t'Kint de Roodenbeke, C., Kaplan, M. D., Low, D. A., and Hayes, C. S. (2013) Rhs proteins from diverse bacteria mediate intercellular competition. *Proc. Natl. Acad. Sci. U.S.A.* **110,** 7032–7037
7. Russell, A. B., LeRoux, M., Hathazi, K., Agnello, D. M., Ishikawa, T., Wiggins, P. A., Wai, S. N., and Mougous, J. D. (2013) Diverse type VI secretion phospholipases are functionally plastic antibacterial effectors. *Nature* **496,** 508–512
8. Miyata, S. T., Kitaoka, M., Brooks, T. M., McAuley, S. B., and Pukatzki, S. (2011) Vibrio cholerae requires the type VI secretion system virulence factor VasX to kill *Dictyostelium discoideum*. *Infect. Immun.* **79,** 2941–2949
9. Russell, A. B., Singh, P., Brittnacher, M., Bui, N. K., Hood, R. D., Carl, M. A., Agnello, D. M., Schwarz, S., Goodlett, D. R., Vollmer, W., and Mougous, J. D. (2012) A widespread bacterial type VI secretion effector superfamily identified using a heuristic approach. *Cell Host Microbe* **11,** 538–549
10. Chou, S., Bui, N. K., Russell, A. B., Lexa, K. W., Gardiner, T. E., LeRoux, M., Vollmer, W., and Mougous, J. D. (2012) Structure of a peptidoglycan amidase effector targeted to Gram-negative bacteria by the type VI secretion system. *Cell reports* **1,** 656–664
11. Brooks, T. M., Unterweger, D., Bachmann, V., Kostiuk, B., and Pukatzki, S. (2013) Lytic activity of the *Vibrio cholerae* type VI secretion toxin VgrG-3 is inhibited by the antitoxin TsaB. *J. Biol. Chem.* **288,** 7618–7625
12. English, G., Trunk, K., Rao, V. A., Srikannathasan, V., Hunter, W. N., and Coulthurst, S. J. (2012) New secreted toxins and immunity proteins encoded within the type VI secretion system gene cluster of *Serratia marcescens*. *Mol. Microbiol.* **86,** 921–936
13. Zhang, H., Zhang, H., Gao, Z. Q., Wang, W. J., Liu, G. F., Xu, J. H., Su, X. D., and Dong, Y. H. (2013) Structure of the type VI effector-immunity complex (Tae4-Tai4) provides novel insights into the inhibition mechanism of the effector by its immunity protein. *J. Biol. Chem.* **288,** 5928–5939
14. Dong, C., Zhang, H., Gao, Z. Q., Wang, W. J., She, Z., Liu, G. F., Shen, Y. Q., Su, X. D., and Dong, Y. H. (2013) Structural insights into the inhibition of type VI effector Tae3 by its immunity protein Tai3. *Biochem. J.* **454,** 59–68
15. Ding, J., Wang, W., Feng, H., Zhang, Y., and Wang, D. C. (2012) Structural insights into the *Pseudomonas aeruginosa* type VI virulence effector Tse1 bacteriolysis and self-protection mechanisms. *J. Biol. Chem.* **287,** 26911–26920
16. Dong, T. G., Ho, B. T., Yoder-Himes, D. R., and Mekalanos, J. J. (2013) Identification of T6SS-dependent effector and immunity proteins by Tn-seq in *Vibrio cholerae*. *Proc. Natl. Acad. Sci. U.S.A.* **110,** 2623–2628
17. Loper, J. E., Hassan, K. A., Mavrodi, D. V., Davis, E. W., 2nd, Lim, C. K., Shaffer, B. T., Elbourne, L. D., Stockwell, V. O., Hartney, S. L., Breakwell, K., Henkels, M. D., Tetu, S. G., Rangel, L. I., Kidarsa, T. A., Wilson, N. L., van de Mortel, J. E., Song, C., Blumhagen, R., Radune, D., Hostetler, J. B., Brinkac, L. M., Durkin, A. S., Kluepfel, D. A., Wechter, W. P., Anderson, A. J., Kim, Y. C., Pierson, L. S., 3rd, Pierson, E. A., Lindow, S. E., Kobayashi, D. Y., Raaijmakers, J. M., Weller, D. M., Thomashow, L. S., Allen, A. E., and Paulsen, I. T. (2012) Comparative genomics of plant-associated *Pseudomonas* spp.: insights into diversity and inheritance of traits involved in multitrophic interactions. *PLoS Genet.* **8,** e1002784
18. Fritsch, M. J., Trunk, K., Alcoforado Diniz, J., Guo, M., Trost, M., and Coulthurst, S. J. (2013) Proteomic identification of novel secreted antibacterial toxins of the *Serratia marcescens* Type VI secretion system. *Mol. Cell. Proteomics* [Epub ahead of print]
19. Kelley, L. A., and Sternberg, M. J. (2009) Protein structure prediction on the Web: a case study using the Phyre server. *Nat. Protoc.* **4,** 363–371
20. Paulsen, I. T., Press, C. M., Ravel, J., Kobayashi, D. Y., Myers, G. S., Mav-

rodi, D. V., DeBoy, R. T., Seshadri, R., Ren, Q., Madupu, R., Dodson, R. J., Durkin, A. S., Brinkac, L. M., Daugherty, S. C., Sullivan, S. A., Rosovitz, M. J., Gwinn, M. L., Zhou, L., Schneider, D. J., Cartinhour, S. W., Nelson, W. C., Weidman, J., Watkins, K., Tran, K., Khouri, H., Pierson, E. A., Pierson, L. S., 3rd, Thomashow, L. S., and Loper, J. E. (2005) Complete genome sequence of the plant commensal *Pseudomonas fluorescens* Pf-5. *Nat. Biotechnol.* **23,** 873–878

21. Mougous, J. D., Cuff, M. E., Raunser, S., Shen, A., Zhou, M., Gifford, C. A., Goodman, A. L., Joachimiak, G., Ordoñez, C. L., Lory, S., Walz, T., Joachimiak, A., and Mekalanos, J. J. (2006) A virulence locus of *Pseudomonas aeruginosa* encodes a protein secretion apparatus. *Science* **312,** 1526–1530
22. Hassan, K. A., Johnson, A., Shaffer, B. T., Ren, Q., Kidarsa, T. A., Elbourne, L. D., Hartney, S., Duboy, R., Goebel, N. C., Zabriskie, T. M., Paulsen, I. T., and Loper, J. E. (2010) Inactivation of the GacA response regulator in *Pseudomonas fluorescens* Pf-5 has far-reaching transcriptomic consequences. *Environ. Microbiol.* **12,** 899–915
23. Goodman, A. L., Kulasekara, B., Rietsch, A., Boyd, D., Smith, R. S., and Lory, S. (2004) A signaling network reciprocally regulates genes associated with acute infection and chronic persistence in *Pseudomonas aeruginosa*. *Dev. Cell* **7,** 745–754
24. Nelson, K. E., Weinel, C., Paulsen, I. T., Dodson, R. J., Hilbert, H., Martins dos Santos, V. A., Fouts, D. E., Gill, S. R., Pop, M., Holmes, M., Brinkac, L., Beanan, M., DeBoy, R. T., Daugherty, S., Kolonay, J., Madupu, R., Nelson, W., White, O., Peterson, J., Khouri, H., Hance, I., Chris Lee, P., Holtzapple, E., Scanlan, D., Tran, K., Moazzez, A., Utterback, T., Rizzo, M., Lee, K., Kosack, D., Moestl, D., Wedler, H., Lauber, J., Stjepandic, D., Hoheisel, J., Straetz, M., Heim, S., Kiewitz, C., Eisen, J. A., Timmis, K. N., Düsterhöft, A., Tümmler, B., and Fraser, C. M. (2002) Complete genome sequence and comparative analysis of the metabolically versatile *Pseudomonas putida* KT2440. *Environ. Microbiol.* **4,** 799–808
25. Choi, K. H., Gaynor, J. B., White, K. G., Lopez, C., Bosio, C. M., Karkhoff-Schweizer, R. R., and Schweizer, H. P. (2005) A Tn7-based broad-range bacterial cloning and expression system. *Nat. Methods* **2,** 443–448
26. Lambertsen, L., Sternberg, C., and Molin, S. (2004) Mini-Tn7 transposons for site-specific tagging of bacteria with fluorescent proteins. *Environ. Microbiol.* **6,** 726–732
27. MacDowell, A. A., Celestre, R. S., Howells, M., McKinney, W., Krupnick, J., Cambie, D., Domning, E. E., Duarte, R. M., Kelez, N., Plate, D. W., Cork, C. W., Earnest, T. N., Dickert, J., Meigs, G., Ralston, C., Holton, J. M., Alber, T., Berger, J. M., Agard, D. A., and Padmore, H. A. (2004) Suite of three protein crystallography beamlines with single superconducting bend magnet as the source. *J. Synchrotron Radiat.* **11,** 447–455
28. Winter, G. (2010) *xia2*: an expert system for macromolecular crystallography data reduction. *J. Appl. Crystallogr.* **43,** 186–190
29. Terwilliger, T. C., Adams, P. D., Read, R. J., McCoy, A. J., Moriarty, N. W., Grosse-Kunstleve, R. W., Afonine, P. V., Zwart, P. H., and Hung, L. W. (2009) Decision-making in structure solution using Bayesian estimates of map quality: the PHENIX AutoSol wizard. *Acta Crystallogr. D Biol. Crystallogr.* **65,** 582–601
30. Terwilliger, T. C., Grosse-Kunstleve, R. W., Afonine, P. V., Moriarty, N. W., Zwart, P. H., Hung, L. W., Read, R. J., and Adams, P. D. (2008) Iterative model building, structure refinement and density modification with the PHENIX AutoBuild wizard. *Acta Crystallogr. D Biol. Crystallogr.* **64,** 61–69
31. Emsley, P., Lohkamp, B., Scott, W. G., and Cowtan, K. (2010) Features and development of Coot. *Acta Crystallogr. D Biol. Crystallogr.* **66,** 486–501
32. Afonine, P. V., Grosse-Kunstleve, R. W., Echols, N., Headd, J. J., Moriarty, N. W., Mustyakimov, M., Terwilliger, T. C., Urzhumtsev, A., Zwart, P. H., and Adams, P. D. (2012) Towards automated crystallographic structure refinement with phenix.refine. *Acta Crystallogr. D Biol. Crystallogr.* **68,** 352–367
33. Vollmer, W., Joris, B., Charlier, P., and Foster, S. (2008) Bacterial peptidoglycan (murein) hydrolases. *FEMS Microbiol. Rev.* **32,** 259–286
34. Weaver, L. H., Grütter, M. G., and Matthews, B. W. (1995) The refined structures of goose lysozyme and its complex with a bound trisaccharide show that the "goose-type" lysozymes lack a catalytic aspartate residue. *J. Mol. Biol.* **245,** 54–68
35. Kuroki, R., Weaver, L. H., and Matthews, B. W. (1993) A covalent enzyme-substrate intermediate with saccharide distortion in a mutant T4 lysozyme. *Science* **262,** 2030–2033
36. Kuroki, R., Weaver, L. H., and Matthews, B. W. (1995) Structure-based design of a lysozyme with altered catalytic activity. *Nat. Struct. Biol.* **2,** 1007–1011
37. Deflaun, M. F., Marshall, B. M., Kulle, E. P., and Levy, S. B. (1994) Tn5 insertion mutants of *Pseudomonas fluorescens* defective in adhesion to soil and seeds. *Appl. Environ. Microbiol.* **60,** 2637–2642
38. Rodríguez-Herva, J. J., Reniero, D., Galli, E., and Ramos, J. L. (1999) Cell envelope mutants of *Pseudomonas putida*: physiological characterization and analysis of their ability to survive in soil. *Environ. Microbiol.* **1,** 479–488
39. Holm, L., and Rosenström, P. (2010) Dali server: conservation mapping in 3D. *Nucleic acids research* **38,** W545–549
40. Hashimoto, W., Ochiai, A., Momma, K., Itoh, T., Mikami, B., Maruyama, Y., and Murata, K. (2009) Crystal structure of the glycosidase family 73 peptidoglycan hydrolase FlgJ. *Biochem. Biophys. Res. Commun.* **381,** 16–21
41. Bublitz, M., Polle, L., Holland, C., Heinz, D. W., Nimtz, M., and Schubert, W. D. (2009) Structural basis for autoinhibition and activation of Auto, a virulence-associated peptidoglycan hydrolase of *Listeria monocytogenes*. *Mol. Microbiol.* **71,** 1509–1522
42. Gérard, F., Brooks, M. A., Barreteau, H., Touzé, T., Graille, M., Bouhss, A., Blanot, D., van Tilbeurgh, H., and Mengin-Lecreulx, D. (2011) X-ray structure and site-directed mutagenesis analysis of the *Escherichia coli* colicin M immunity protein. *J. Bacteriol.* **193,** 205–214
43. El Ghachi, M., Bouhss, A., Barreteau, H., Touzé, T., Auger, G., Blanot, D., and Mengin-Lecreulx, D. (2006) Colicin M exerts its bacteriolytic effect via enzymatic degradation of undecaprenyl phosphate-linked peptidoglycan precursors. *J. Biol. Chem.* **281,** 22761–22772
44. Krissinel, E., and Henrick, K. (2007) Inference of macromolecular assemblies from crystalline state. *J. Mol. Biol.* **372,** 774–797
45. Abergel, C., Monchois, V., Byrne, D., Chenivesse, S., Lembo, F., Lazzaroni, J. C., and Claverie, J. M. (2007) Structure and evolution of the Ivy protein family, unexpected lysozyme inhibitors in Gram-negative bacteria. *Proc. Natl. Acad. Sci. U.S.A.* **104,** 6394–6399
46. Yum, S., Kim, M. J., Xu, Y., Jin, X. L., Yoo, H. Y., Park, J. W., Gong, J. H., Choe, K. M., Lee, B. L., and Ha, N. C. (2009) Structural basis for the recognition of lysozyme by MliC, a periplasmic lysozyme inhibitor in Gram-negative bacteria. *Biochem. Biophys. Res. Commun.* **378,** 244–248
47. Leysen, S., Vanderkelen, L., Weeks, S. D., Michiels, C. W., and Strelkov, S. V. (2013) Structural basis of bacterial defense against g-type lysozyme-based innate immunity. *Cell. Mol. Life Sci.* **70,** 1113–1122
48. Thunnissen, A. M., Rozeboom, H. J., Kalk, K. H., and Dijkstra, B. W. (1995) Structure of the 70-kDa soluble lytic transglycosylase complexed with bulgecin A. Implications for the enzymatic mechanism. *Biochemistry* **34,** 12729–12737
49. Vollmer, W. (2008) Structural variation in the glycan strands of bacterial peptidoglycan. *FEMS Microbiol. Rev.* **32,** 287–306
50. De Las Rivas, B., García, J. L., López, R., and García, P. (2002) Purification and polar localization of pneumococcal LytB, a putative endo-β-*N*-acetylglucosaminidase: the chain-dispersing murein hydrolase. *Journal of bacteriology* **184,** 4988–5000
51. Fox, J. M., Jess, P., Jambusaria, R. B., Moo, G. M., Liphardt, J., Clark, D. S., and Blanch, H. W. (2013) A single-molecule analysis reveals morphological targets for cellulase synergy. *Nat. Chem. Biol.* **9,** 356–361
52. Chen, V. B., Arendall, W. B., 3rd, Headd, J. J., Keedy, D. A., Immormino, R. M., Kapral, G. J., Murray, L. W., Richardson, J. S., and Richardson, D. C. (2010) MolProbity: all-atom structure validation for macromolecular crystallography. *Acta Crystallogr. D Biol. Crystallogr.* **66,** 12–21
53. Adams, P. D., Afonine, P. V., Bunkóczi, G., Chen, V. B., Davis, I. W., Echols, N., Headd, J. J., Hung, L. W., Kapral, G. J., Grosse-Kunstleve, R. W., McCoy, A. J., Moriarty, N. W., Oeffner, R., Read, R. J., Richardson, D. C., Richardson, J. S., Terwilliger, T. C., and Zwart, P. H. (2010) PHENIX: a comprehensive Python-based system for macromolecular structure solution. *Acta Crystallogr. D Biol. Crystallogr.* **66,** 213–221